Advances in Applied Ceramics: Structural, Functional and Bioceramics

One-dimensional steady-state thermal model for rotary kilns used in the manufacture of cement

--Manuscript Draft--

Manuscript Number:	AAC1727R1
Full Title:	One-dimensional steady-state thermal model for rotary kilns used in the manufacture of cement
Article Type:	Research paper
Keywords:	Rotary kiln; Heat transfer; Cement; Clinker; Thermal model; Steady state
Corresponding Author:	Theodore Hanein University of Sheffield Sheffield, UNITED KINGDOM
Corresponding Author Secondary Information:	
Corresponding Author's Institution:	University of Sheffield
Corresponding Author's Secondary Institution:	
First Author:	Theodore Hanein
First Author Secondary Information:	
Order of Authors:	Theodore Hanein
	Fred P Glasser
	Marcus Nigel Bannerman
Order of Authors Secondary Information:	
Abstract:	Rotary kilns are used extensively in the cement industry to convert raw meal into cement clinker. In order to optimize the operation of cement kilns, computationally efficient thermal models are required. In this work, the development of a one-dimensional thermal model for kilns is explored. To simplify the model, the kiln is assumed to be well mixed in the transverse direction. A simultaneous mass and energy balance is solved based on a steady-state approximation. Existing semi-empirical models for heat transfer in the kiln are implemented and critically evaluated. The resulting one-dimensional model is capable of predicting axial temperature profiles in the rotary kiln which agree well with the available experimental data found in the literature. The model presented extends from previous models by considering a full enthalpy balance for the gas in the kiln. This allows the model to be used in a fully predictive manner, taking into account the temperature-dependent thermodynamic, transport, and radiative properties of the gas phase.

Dear editor and reviewer:

Thank you for your feedback and consideration of our work for publication. This letter contains in-line response (in red font) to your comments. The changes in the text document are also in red font as requested. Some changes to the document not relating to the reviewers comments have also been made; these are:

Pg1Ln2: The title has been changed in order to more clearly describe the content of the paper.

Table 3: Values have changed slightly due to a minor mistake found in the programming code after submission. The new values reported are based on calculations after correction.

Supplementary material 5: This material has been removed as they are superfluous. They are not needed to repeat the simulations.

Section numbers of conclusions and acknowledgement have been corrected; section number “5” was repeated in the initial submission.

Pg6Ln36: Boltzmann was spelled incorrectly and is now corrected.

For consistency throughout the paper, all subscripts “amb” in all equations have been changed to “ext”(external).

Reference numbering has been corrected.

Typographical errors have been corrected in the document “Supplementary material summary”. The correction is from “degrees Celsius” to “Kelvin” x 2.

Figure 2 has been corrected. Previous submitted image was labelled degrees Celsius but was mistakenly plotted in Kelvin.

A new figure has been added to provide an example of the model works on the Tscheng kiln.

In order to better organize the supplementary material, the data in supplementary material 4 have been transposed.

Comments from the Editors and Reviewers:

Reviewer #1: This paper describes a computational model of heat transfer within a rotary kiln. The authors state that it can be developed to provide predictive performance modeling of kiln operations with a target of improving production efficiency of the cement industry. The paper is well written and provides a concise explanation of the derivation of the energy balance equation forming the basis of the model.

Thank you for your kind remarks.

Reviewer Comments

Pg5Ln1. An assumption is made of constant gas velocity for the model, but in Supplementary Material 2 of experimental data of the Barr pilot kiln experiments there are data columns for "primary" and "secondary" air flow rate. Is this impactful to the average error values reported?

No, this should not impact the average error of the values. The rate for air used in our calculations is the sum of the “primary” and “secondary”. This has now also been clarified in the text in the first paragraph of section 4. Thank you.

Pg5Ln30. An inconsistency in the citation of referencing is noted. At this point in the text "…Ref. XX" is used, while later (Pg6Ln53) "…Ref. [XX]" is used. It's suggested that picking one format for the entirety of the paper will prove to be clearer.

Thank you for spotting this; we have now corrected the referencing.

Pg6Ln48. The authors state that the value of the gas film thickness has an optimum value of 0.1 for sand particles between approximately 150 microns and 1mm (which is hopefully consistent with the gradation of "Ottawa sand" referenced in the following paragraph although not stated in the text). As the targeted application of this paper is the cement industry - for which the clinkerization process may start with fine powder but develop into larger (>1mm) clinker granules, with a possible melt phase occurring along the length of the kiln - could the authors provide some context as to how the gas film thickness will vary in a cement rotary kiln?

The particle size diameter is provided in the text; for the Tscheng experiments as stated on in the second paragraph of section 4 as follows:

"In addition to the data files, the remaining information required to reproduce this work which is not provided in the supplementary material is that the solid particle diameter of all the Tscheng trials was 0.73 mm"

Also, the particle size diameter for the Barr experiments is provided in Supplementary Material 2.

Further experiments would need to be carried out to find the effect of the growing clinker nodules. i.e., the clinker particle size as a function of temperature would need to be evaluated. A new optimum can then be deduced for cement kilns or a fit produced and used to input gas film thickness as a function of particle size.

Pg8Ln49. The sentence "It is a major industrial concern and energy efficiency one of the primary focuses of current research…", may read clearer if amended to "It is a major industrial concern and energy efficiency is one of the primary focuses of current research…".

Thank you; this has now been changed.

Title:
One-dimensional steady-state thermal model for rotary kilns used in the manufacture of cement

Authors:
Theodore **Hanein**[1]**,** Fred P. **Glasser**[2]**,** and Marcus N. **Bannerman**[1]

Affiliation:
[1]*School of Engineering, University of Aberdeen, AB24 3UE, United Kingdom*
[2]*Department of Chemistry, University of Aberdeen, AB24 3UE, United Kingdom*

First author: Theodore Hanein. Email address: theodorehanein@gmail.com. Postal address: Fraser Noble Building, School of Engineering, King's College, University of Aberdeen, Aberdeen, AB24 3UE, United Kingdom. Tel: +44 (0) 7824862590.

Second author: Fred P. Glasser. Email address: f.p.glasser@abdn.ac.uk. Postal address: Meston Building, Meston Walk, University of Aberdeen, Aberdeen, AB243UE, United Kingdom. Tel: +44 (0) 122427906

Corresponding author: Marcus N. Bannerman. Email address: m.campbellbannerman@abdn.ac.uk. Postal address: Fraser Noble Building, School of Engineering, King's College, University of Aberdeen, Aberdeen, AB24 3UE, United Kingdom. Tel: +44 (0) 1224 274480.

Abstract
Rotary kilns are used extensively in the cement industry to convert raw meal into cement clinker. In order to optimize the operation of cement kilns, computationally efficient thermal models are required. In this work, the development of a one-dimensional thermal model for kilns is explored. To simplify the model, the kiln is assumed to be well mixed in the transverse direction. A simultaneous mass and energy balance is solved based on a steady-state approximation. Existing semi-empirical models for heat transfer in the kiln are implemented and critically evaluated. The resulting one-dimensional model is capable of predicting axial temperature profiles in the rotary kiln which agree well with the available experimental data found in the literature. The model presented here extends from previous published models by considering a full enthalpy balance for the gas in the kiln. This allows the model to be used in a fully predictive manner, taking into account the temperature-dependent thermodynamic, transport, and radiative properties of the gas phase.

Keywords*: Rotary kiln, heat transfer, cement, clinker, thermal model*

List of symbols

Symbols

α	(dimensionless)	Absorptivity
Ω	(rad s^{-1})	Angular velocity of kiln
h_b	(m)	Bed height
Φ	(dimensionless)	Bed solid volume fraction
θ	(rad)	Central angle formed by the solid bed
L_c	(m)	Chord length of the solid bed

ρ	(kg m^{-3})	Density
μ	(kg $m^{-1}s^{-1}$)	Dynamic viscosity
ε	(dimensionless)	Emissivity
F	(dimensionless)	Form/view factor
χ	(dimensionless)	Gas film thickness
Gr	(dimensionless)	Grashof number
Q	(W m^{-1})	Heat flux per unit length
h	(W m^{-2} K^{-1})	Heat transfer coefficient
D_h	(m)	Hydraulic diameter
C_p	(kJ kg^{-1} K^{-1})	Isobaric heat capacity
D	(m)	Kiln inner diameter
D_o	(m)	Kiln outer diameter
η	(dimensionless)	Kiln solid loading fraction
$\dot{m}$	(kg s^{-1})	Mass flow rate
L_m	(m^{-1})	Mean beam length
Nu	(dimensionless)	Nusselt number
d_p	(m)	Particle diameter
P	(m)	Perimeter for heat transfer
Pr	(dimensionless)	Prandtl number
Ra	(dimensionless)	Rayleigh number
σ	(W m^{-2} K^{-4})	Stefan Boltzmann constant
T	(K)	Temperature
k	(W m^{-1} K^{-1})	Thermal conductivity
R	(m^2 K W^{-1})	Thermal resistance
v	(m s^{-1})	Velocity

Superscripts and Subscripts

an	Angular
ax	Axial
b	Bulk bed
cd	Conduction
cv	Convection
cw	Covered wall
ext	External
g	Gas
j	j^{th} kiln wall layer
rd	Radiation
sh	Shell
s	Solid bed
w	Wall

1. Introduction

Rotary kilns are crucial processing units in the chemical, metallurgical, and pharmaceutical industries. The rotary kiln is popular as it is the most advanced high-throughput and high-temperature industrial kiln technology. It is also the preferred choice in cement manufacture where production rates approach kilotons per day and many of the critical reactions take place at temperatures up to 1500°C. The world demand for cement is on the increase and at present the cement industry consumes approximately 12–15% of the global industrial energy

demand.[1] The cement industry also emits approximately 5–8% of global CO_2 emissions which arise from the decomposition of limestone and the combustion of fuels.[2,3] It is therefore vital that kilns are well understood to allow the optimization of heat-transfer in existing kiln installations. In addition, it is essential that detailed models for the kiln are available so that novel low-carbon cement formulations can be designed and developed. Finally, to enable effective scale-up of lab based processes to pilot or industrial scales it is crucial that the conditions within the kiln are well characterized.

Unfortunately, the conditions within a kiln are not homogeneous and there is a complex relationship between the reactions, mass transfer, heat transfer, and mechanical dynamics of the processed material. Despite these difficulties, existing literature has focused on creating one-dimensional models which can capture quantitatively the kiln operation while remaining computationally tractable for optimization studies. A coarse-grained computational model which is capable of predicting the thermal performance of the kiln within seconds is essential to enable plant-wide process optimization.

Li et al.[4] were one of the first to develop a simple full-kiln heat-transfer model while developing an extended penetration theory to model the wall-bed heat transfer within unreactive rotary kilns. Mujumdar and Ranade[5] also developed a one dimensional model where they use a simple kinetic model to approximate reactions within the kiln. It should be noted that including a detailed kinetic model is extremely difficult as not all chemical reactions occurring in the cement production process are known, nor is the kinetic data available. Finally, Romero Valle[6] developed a heat transfer model which combines the two aforementioned studies and the model presented here is based on that work. The models introduced predict the temperatures of the solid bed, the wall, and the outer shell. The work presented here improves on these previous works by also calculating the gas-phase temperature and considers accurate temperature-dependent thermodynamic descriptions of the solid and gas phases within the kiln. These improvements allow the model to be used in a fully predictive manner without measuring the gas temperatures of the target kiln during operation. There are commercial kiln models available which go beyond many of the approximations within this study, e.g. KilnSimu;[7] however, the detailed implementation of these models is not yet widely available. As this study aims to validate the performance of current heat-transfer models for kilns, it is tested against the full range of available experimental data for inert beds from Barr[8] and Tscheng[9], whereas previous studies have only used a limited subset of this data. The Tscheng kiln is shorter (2.44 m) than the Barr kiln (5.5 m) and is operated at lower temperatures. This difference in operation allows a closer evaluation of the convective and radiative transport models. The experimental data used here has been carefully compiled and, where required, digitized from the original sources and the resulting data files are available in the supplementary material to support further development in this field.

In the following two sections the kiln model is outlined and its approximations are discussed. Section 4 validates the model against the available experimental data before the conclusions are presented in Sec. 5.

2. Mass balance

In conventional cement manufacture, the kiln is operated as a combined counter-current heat exchanger and reactor. As illustrated in Fig. 1, the solid phases enter at the cold end of the kiln and travel towards the burner while the gas phase flows in the opposite direction. In this study, only experiments with unreactive beds are considered to allow a detailed examination

of the thermal model. As such, there is no interchange of mass between phases and compositions can be assumed to remain constant along the length of the kiln. Pressure drop is also ignored along the kiln resulting in a constant gas velocity. In addition, the experimental studies considered here were carried out carefully to ensure a relatively constant bed height along the length of the kiln.[8,9] This originally facilitated the development of the kiln heat transfer models and allows this study to isolate and validate the performance of these models within a more complete description of the kiln.

3. Energy balance

A one-dimensional model for inert constant-bed-height kilns can be constructed by performing a differential enthalpy balance over a transverse slice of the kiln. Within each slice, the solid and gas phases are treated as separate but homogeneous thermal bodies at a temperature T_s and T_g respectively. Assuming steady state, separate enthalpy balances for the solid and gas phases yield the following differential equations,

$$\dot{m}_s C_{p,s} \frac{\delta T_s}{\delta x} = Q^{cv}_{g\to s} + Q^{cd}_{w\to s} + Q^{rd}_{g\to s} + Q^{rd}_{w\to s} \qquad \textbf{(Eq. 1)}$$

$$\dot{m}_g C_{p,g} \frac{\delta T_g}{\delta x} = -\left(Q^{cv}_{g\to s} + Q^{cv}_{g\to w} + Q^{rd}_{g\to s} + Q^{rd}_{g\to w}\right), \qquad \textbf{(Eq. 2)}$$

where C_p is the isobaric heat capacity, $\dot{m}$ is the mass flux, and Q is a heat flux per unit length of the kiln at the current distance, x, along the kiln. On the heat flux terms, the superscripts indicate convective (cv), radiative (rd), or conductive (cd) terms whereas the subscripts indicate the phases exchanging heat and the corresponding sign convention (see Fig. 1). As the bed composition is constant, the heat capacity is only a function of temperature. Gas heat capacity data are taken from Ref. 10 and solid heat capacity data are taken from Ref. 11.

The use of the temperatures T_g and T_s in the balance equations fixes their definition as the temperatures of homogeneous phases which have the same enthalpy as the real phase. It is not immediately apparent that temperatures homogenized in this way are appropriate to use as the driving forces for heat transfer between the phases and surroundings. Assuming constant heat transfer resistances, the linear average of the temperature at the interface of each thermal body is required for conduction and convection calculations while a fourth-order volumetric average of temperature is required for gas radiation calculations: therefore no single homogenized value of the temperature is exactly appropriate. The gas has significant variations in temperature over its volume;[12] however, the results of using first and fourth order averaging of temperature has been found to be numerically close in this case.[13] This study, in-line with previous work,[6] will directly use the homogeneous temperatures in the integrated heat transfer expressions and look to validate this approach as part of the study. It should also be noted that the assumption of a well-mixed solid bed is generally appropriate due to the design of a rotary kiln which promotes transverse mixing and often operates at low solid loadings.[14] The effect of the temperature gradient driving axial conduction is also neglected in this work for simplicity; however, due to the large aspect ratio of kilns (and the solid bed) the error brought about by this assumption is expected to be relatively small.[4]

As part of the calculations of the heat flux, the outer shell and inner wall temperatures are required. Again, for simplicity these bodies are assumed to be homogeneous in temperature which reduces the representative temperature field to a single value and neglects internal effects such as wall to wall radiative heat transfer. At steady state, the internal wall

temperature, T_w, and external shell temperature, T_{sh}, can be solved for implicitly via an energy balance,

$$Q_{w\to ext} = Q^{rd}_{g\to w} + Q^{cv}_{g\to w} - Q^{rd}_{w\to s} - Q^{cd}_{w\to s} \quad \textbf{(Eq. 3)}$$

$$Q_{w\to sh} = Q^{rd}_{g\to w} + Q^{cv}_{g\to w} - Q^{rd}_{w\to s} - Q^{cd}_{w\to s}. \quad \textbf{(Eq. 4)}$$

This set of differential algebraic equations, (1) to (4), is solved simultaneously for each differential slice to calculate the temperatures of the system along the length of the kiln. The solver used here is an implicit differential algebraic solver (Implicit_Problem from Ref. 15) using 30 steps in x, with absolute and relative tolerances both set at 10^{-4}. To complete the model, expressions for the heat fluxes are required and these are described in the following subsections.

3.1. Conduction/Penetration between the solid bed and the kiln internal walls ($Q^{cd}_{w\to s}$)

Heat transfer between the underside of the solid bed and the internal wall which it covers plays an important role in the heat transferred. Although this effect is notionally denoted here as a conductive heat transfer due to the close proximity of the bed and wall, the three dominant mechanisms for heat transfer in this case are actually conduction through the gas film between the wall and the bed, direct solid-wall contact conduction, and advective heat transfer near the bed edges. Older conduction models did not take into account the presence of a gas film;[16,17] however, Lehmberg et al.[18] first included terms for a gas film and presented a complex model which cannot readily be used for design purposes due to its requirement of additional experimental parameters. Tscheng[9] attempted to correlate experimental data[16-18] and proposed a model that is restricted to relatively low temperatures and does not take into account the effect of particle size. Li et al.[4] later extended penetration theory for packed beds and fluidized bed reactors developed by Schluender[19] to describe the heat transfer between the bulk solids and the covered internal wall in a rotary kiln. Their model, validated against experiments,[18,20] presents the heat transfer coefficient as,

$$h^{cd}_{cw\to s} = \frac{\chi d_p}{k_g} + \frac{0.5}{\sqrt{\frac{2k_b\rho_b C_{p,s}\omega}{\theta}}},$$

where χ is a dimensionless thickness of the gas film, d_p is the particle diameter, k is the thermal conductivity, ρ_b is the bulk density, ω is the angular velocity of the kiln, $\theta = 2\sin^{-1}(L_c)/D$ is the central angle formed with the solid bed, D, is the kiln internal diameter, and L_c is the chord length of the solid bed. The gas film thickness, χ, is reported to be in the range of 0.096 – 0.198 for rotary kilns, with an optimum value of 0.1 in rotary kilns as calculated for sand with particles size in the range 0.1575–1.038mm; [4] this value is used in all of our calculations. The temperature-dependent transport properties of the gas phase and the surroundings (discussed later on) such as thermal conductivities and viscosities are taken from Ref. 21. In our model, the effective bed thermal conductivity, k_b, is calculated using the Maxwell model based on effective medium theory as shown below,

$$k_b = \left(\frac{2k_g + k_s + 2\Phi(k_s - k_g)}{2k_g + k_s - \Phi(k_s - k_g)}\right)k_g,$$

where Φ is the bed solid volume fraction. Ottawa sand, which is the solid feed used in all experimental trials considered here, is composed of naturally rounded grains of nearly pure quartz[22] and is here assumed to be 100% quartz. Temperature dependent thermal conductivity data for quartz up to 700K is readily available.[23] Above this temperature, the thermal conductivity is assumed to be constant as suggested by Yoon et al.[24] Solid densities and particle diameters are each taken from the sources of the individual experiments.[8,9] Finally, the heat flux is calculated as follows,

$$Q_{w\to s}^{cd} = h_{cw-s}^{cd} P_{cw-s}\left(T_w - T_s\right),$$

where $P_{cw-s} = \theta D/2$ is the perimeter of the wall in contact with the solid bed.

3.2. Radiation ($Q_{g\to w}^{rd}$, $Q_{w\to s}^{rd}$, $Q_{g\to s}^{rd}$)

The cement kiln enclosure contains a mixture of gases generated from the combustion of fuels and chemical reactions occurring within the kiln. In our simulations, the gas is assumed to be either dry air (see Table 1) or the result of complete combustion of the natural gas in dry air. To achieve an accurate description of radiative heat transfer within the kiln, evaluation of the emissive and absorptive properties of these gas mixtures is required. The procedure of Hottel and Sarofim[25] is followed here using temperature dependent total gas mixture absorptivity and emissivity correlations with linear extrapolation.[26] The emissivity of the surfaces of the bed, wall, and shell are assumed to be standard values reported in literature:[6] 0.9, 0.85, and 0.8 respectively. Due to the complexity involved in accounting for a large series of emissivity relations due to partial and second incidence absorption, reflection and transmission, the radiative heat transfer between the gas and bed or wall are calculated using a simplified radiation model,[25]

$$Q_{g\to s/w}^{rd} = \sigma\left(\varepsilon_{s/w}+1\right)P_{g-s/w}\frac{\varepsilon_g T_g^4 - \alpha_g T_{s/w}^4}{2}, \qquad \textbf{(Eq. 5)}$$

where σ is the Stefan Boltzmann constant, ε is an emissivity, and α is an absorptivity which are both a function of the mean beam length (L_m). The correlation of Gorog et al.[27] is used to calculate the average mean beam length which includes reflection effects: $L_m = 0.95D(1-h_b/D)$ where h_b is the height of the bed. Depending on whether this equation is for the solid or the wall (s/w), the perimeter is either $P_{g-s} = L_c$ (exposed bed) or $P_{g-w} = \pi D - \theta D/2$ (exposed wall). Equation (5) is derived from the expression for the radiative heat transfer rate from a gas to a black surface multiplied by a low-order correction factor, $\left(\varepsilon_{s/w}+1\right)/2$, for the emissivity of the surface. Hottel and Sarofim have shown that if the emissivity of the surface is high ($\varepsilon_{s/w} \geq 0.8$), the error introduced by use of this truncated expression does not exceed 10%.[25] Radiative heat transfer between the internal wall and the solid bed is calculated using the following expression,[25]

$$Q_{w\to s}^{rd} = \frac{\sigma\left(T_w^4 - T_s^4\right)}{\left(1-\varepsilon_w\right)/\varepsilon_w P_{s-w} + 1/F_{s\to w}P_{w-s} + \left(1-\varepsilon_s\right)/\varepsilon_s P_{w-s}},$$

where $F_{s\to w}$ is the bed to wall form/view factor ($F_{s\to w}=1$ for flat beds) and P_{w-s} is the perimeter of the exposed bed, and P_{s-w} is the perimeter of the exposed wall as defined earlier.

It should be noted that both radiative expressions ignore axial radiation for simplicity and computational efficiency. The gas-solid/wall and solid-wall radiation effects are decoupled for simplicity as well. A more detailed model which includes these effects would require additional computational cost which appears not to be justified here.

3.3. Convection ($Q^{cv}_{g\to s}, Q^{cv}_{g\to w}$)

Convective heat transfer in rotary kilns was studied by Tscheng as a function of kiln operating parameters including gas and solid throughput, rotational speed, solid loading, inclination, particle-size, and temperature.[9] The resulting convective heat transfer coefficients are given below,

$$h_{g-s} = 0.46\frac{k_g}{D_h}\mathrm{Re}_{ax}^{0.535}\,\mathrm{Re}_{an}^{0.104}\,\eta^{-0.341}$$

$$h_{g-w} = 1.54\frac{k_g}{D_h}\mathrm{Re}_{ax}^{0.575}\,\mathrm{Re}_{an}^{-0.292},$$

where η is the solid loading (fraction of solid fill) and D_h is the hydraulic diameter which is given below,

$$D_h = \frac{0.5D\left(2\pi - \theta + \sin\theta\right)}{\left(\pi - \frac{\theta}{2} + \sin\frac{\theta}{2}\right)}.$$

Two Reynolds numbers are used to characterize the gas flow within the kiln and are calculated using the following expressions,

$$\mathrm{Re}_{ax} = \frac{\rho_g \nu_g D_h}{\mu_g} \qquad\qquad \mathrm{Re}_{an} = \frac{\rho_g \omega D_h^2}{\mu_g},$$

where μ_g is the gas dynamic viscosity and $\nu_g = 4\dot{m}_\mathrm{g}\rho_g^{-1}\left(D^2(\pi-\theta) + L_c(D-2h_b)\right)^{-1}$ is the gas velocity based on subtracting the area of the bulk bed from the area of the kiln tube. The gas density is calculated from the ideal gas equation. The overall heat flux is then given by $Q^{cv}_{g\to s} = h_{g-s/w}P_{g-s/w}\left(T_g - T_{s/w}\right)$, where P_{g-s} is the perimeter of the exposed bed and P_{g-w} is the perimeter of the exposed wall as defined earlier.

3.4. Heat loss from the kiln ($Q_{w\to ext}, Q_{w\to sh}$)

Rotary kilns are relatively inefficient unit operations with modern industrial kiln thermal efficiencies reported to be as low as 40%.[28] Heat losses from the kiln therefore play an important role in the overall energy balance in the kiln. It is a major industrial concern and energy efficiency is one of the primary focuses of current research in cement manufacture. The heat loss from the kiln internal wall to the surroundings is derived from the total resistance, R_Total,

$$R_{Total} = \sum_j R^{cd}_{wall,j} + \left(\left(R^{cv}_{sh-ext}\right)^{-1} + \left(R^{rd}_{sh-ext}\right)^{-1}\right)^{-1},$$

where resistance arises from conduction through the layers of the kiln wall. These resistances are in series with the external resistances of convection (R^{cv}_{sh-amb}) and radiation (R^{rd}_{sh-amb}) from

the outer shell of the kiln to the surroundings. These resistances are calculated using standard expressions as shown in the equations below,

$$R^{cd}_{wall,j} = \frac{\ln\left(D_{outer,j}/D_{inner,j}\right)}{2\pi k_j}$$

$$R^{rd}_{sh-ext} = \left(P_{sh}\sigma\varepsilon_{sh}\left(T^2_{sh}+T^2_{ext}\right)\left(T_{sh}+T_{ext}\right)\right)^{-1}$$

$$R^{cv}_{sh-ext} = \frac{D_o}{P_{sh}\mathrm{Nu}_{ext}k_{ext}},$$

where D_o is the outer diameter of kiln, $D_{inner/outer,j}$ are the inner/outer diameters of the wall layer j, the subscript ext is used to indicate the environment external to the kiln, $P_{sh} = \pi D$ is the perimeter of the outer shell, and Nu_{ext} is the Nusselt number for natural convection. Standard semi-empirical expressions for natural convection on the outside of horizontal cylinders were taken from Ref. 29; $\mathrm{Nu}_{ext} = n(\mathrm{Gr}\,\mathrm{Pr})^m$, where Gr is the Grashof number, Pr is the Prandtl number, and the coefficients *n* and *m* vary with the Rayleigh number (Gr Pr) as: 0.85 and 0.188 when $10^2 \le \mathrm{Ra} \le 10^4$, 0.48 and 0.25 when $10^4 \le \mathrm{Ra} \le 10^7$, and 0.125 and 1/3 when $10^7 \le \mathrm{Ra} \le 10^{12}$ respectively. Thermal conductivities of the kiln layers in the Barr kiln are taken from the original source, while those of the Tscheng kiln are assumed to be standard values reported in literature: 0.294 $\mathrm{Wm^{-1}K^{-1}}$ for the refractory, 45.2 $\mathrm{Wm^{-1}K^{-1}}$ for the steel shell, 0.08 $\mathrm{Wm^{-1}K^{-1}}$ for the ceramic paper insulation, and 0.04 $\mathrm{Wm^{-1}K^{-1}}$ for the fibre glass insulation. The heat loss from the kiln to the surroundings is then solved using $Q_{w\to ext} = \left(T_w - T_{ext}\right)/R_{Total}$ and $Q_{w\to sh} = \left(T_w - T_{sh}\right)/\sum_j R^{cd}_{wall,j}$. These equations allow T_w and T_{sh} to be solved for implicitly in each transverse slice using equations (3) and (4).

4. Model Validation

The thermal model described above is validated against experiments which were carried out in two kilns whose physical properties are shown in Table 2. Due to unquantifiable disturbances near the ends of the kilns, only selected regions of the axial length of the kiln are used for validation and these are between 0.8–5.0 m for the Barr kiln[8] and 1.25–1.78 m for the Tscheng kiln.[9] The Tscheng kiln experimental data is extracted from Ref. 9 while the original Barr kiln experimental data is collected via graphical digitization from Ref. 8. The kiln atmosphere in the Tscheng kiln was composed of preheated air while that of the Barr kiln is calculated from the combustion of natural gas in air as described in Ref. 8; for simplicity, the natural gas is assumed to be 100% CH_4. For the Barr kiln calculations; the air flowrate is the sum of the primary and secondary air reported in Ref. 8.

Barr collected two sets of gas temperature measurements, the first set is 2.5 cm above the solid bed surface and the second set is 10 cm away from the kiln wall surface. The latter gas temperatures are used for validation as they appear to be the best available representation of the enthalpy-averaged gas temperature used in the simulation model. The operating conditions of the Tscheng (Supplementary Material 1) and Barr (Supplementary Material 2) kiln trials are provided here. The compiled experimental data for temperature versus kiln length of the Tscheng[8] (Supplementary Material 3) and Barr[8] (Supplementary Material 4) trials are also provided as supplementary data. In addition to the data files, the remaining information required to reproduce this work which is not provided in the supplementary material is that

the solid particle diameter of all the Tscheng trials was 0.73 mm,[9] and in the Barr trials, solid loading was always at 12%, and the kiln RPM at 1.5.[8] In our calculations, the only remaining free parameters are the initial conditions for the solid and gas temperatures. In this case, the temperatures of the solid and gas at the solid inlet end of the kiln then are calculated via least-squares regression of the model results to the kiln data. This is performed as there is insufficient data to determine these values directly from the experiments due to the disturbances at the kiln entry and exit.

The model is compared against 53 sets of kiln trial data and a summary of the simulation predictions is given in Table 3. A representative example of one Barr trial is given in Fig. 2 and a representative example of one Tscheng trial is given in Fig. 3. For the simulation of the Tscheng trial shown in Fig. 3, as the physical properties between 1.02 – 1.22m are not known. Due to the unknown properties of the equipment installed in this region, the initial conditions on both sides of this zone are calculated separately. Table 3 and Figs. 2 and 3 demonstrate that the model gives an excellent agreement between the experimental and simulated temperatures with an average error of ±15.5 K in the Barr kiln and ±6.5 K in the Tscheng kiln. The average absolute error in the Tscheng kiln is significantly lower than that of the Barr kiln; however, the relative errors are comparable due to the lower operating temperatures of the Tscheng experiments. Overall it appears that this model is sufficiently accurate to capture the performance of these two trial kilns. Due to the relatively large difference in operating conditions between the two kiln trial data sets, the strong agreement indicates that this model is quite general and may be capable of predictively capturing the performance of a wide range of kiln geometries and operating conditions.

Figure 4 displays the simulated heat fluxes of the various heat transfer paths for the same selected Barr trial as presented in Fig. 2. It is apparent that the radiative heat flux between the solid bed and the kiln wall is negligible compared to other heat fluxes. A temperature cross-over between the solid and wall implies that the wall heats the solid feed up until around 2 m into the kiln. Figure 5 presents a comparison between the total calculated radiative and convective heat transfer from the gas phase in Barr trial T4. As is expected, convection is dominant at lower temperatures (< 950°C or 2 m into the kiln in this case) and radiation is the dominant at higher temperatures.

The model can also be used to validate the assumptions made by Tscheng[9] in deriving the convective heat transfer coefficients. The radiative contribution calculated from this model is less than 1.5% of the convective contribution in the Tscheng experiments. This approaches the experimental error and validates their assumption to neglect radiation while developing convective heat transfer models for rotary kilns under their conditions.

5. Conclusions

A one dimensional rotary kiln thermal model is presented which considers a full mass and energy balance for all the species of gas and solid in the kiln. The model considers solid and gas temperature-dependent thermodynamic, transport, and radiative properties. The model is demonstrated to predict axial temperature in the rotary kiln to within experimental error, hence validating the key approximations used, such as the homogenization of the temperature. This also appears to confirm that neglecting axial effects is not unreasonable, although these effects may have been partially included during the fitting of the empirical expressions used for heat transfer. By including a thermodynamic description of the gas phase, the model is complete and may be used to predict the performance of new kiln designs (with inert beds). In this case, estimates for the two initial conditions (which are the only free parameters in the

model) may be obtained from an adiabatic flame temperature calculation for the gas inlet and ambient temperature used for the solid inlet. The current model does not include the effects of a burner within the kiln; thus further work will be required to determine the additional radiation effects and progression of combustion along the length of the kiln.

In order to expedite the development of novel clinker compositions and kiln processes such as that in Ref. 30, work is currently underway to couple the thermal model presented here with a thermodynamic database for combustion and cements which we recently compiled.[31] This development will allow the enthalpy of solid and gas reactions to be included in the heat balance and extend the model to reactive systems. There is limited data for the solid phase reaction kinetics; however, our initial results indicate that a simple equilibrium thermodynamic model is capable of predicting the final output of industrial and pilot cement kilns to a reasonable degree of accuracy. Finally, variations in bed height and solid mass flux arising from changes in the solid phase will require a predictive model for the motion of the solid bed; however, there are a number of models available in the literature. The resulting coupled heat transfer, thermodynamics, and solid dynamics model will allow the broad optimization of the kiln design, fuel, and raw feed composition for a wide range of industries.

6. Acknowledgements

The authors gratefully acknowledge the financial support provided by the Gulf Organization for Research and Development (GORD), Qatar through research grant number ENG016RGG11757.

7. References

1. N. A. Madlool, R. Saidur, M. S. Hossain and N. A. Rahim: 'A critical review on energy use and savings in the cement industries', Renew. Sust. Energ. Rev., 2010, **15**, (4), 2042–2060.
2. T. Hanein, M. S. Imbabi, F. P. Glasser, and M. N. Bannerman. Lowering the carbon footprint and energy consumption of cement production: A novel Calcium SulfoAluminate cement production process. In: Proceedings of the 1st International Conference on Grand Challenges in Construction Materials; 2016 Mar 17-18; Los Angeles, CA: University of California.
3. J. GJ. Olivier, G. Janssens-Maenhout, M. Muntean, and J. A. H. W. Peters: 'Trends in global CO_2 emissions: 2015 Report', PBL Netherlands Environmental Assessment Agency, The Hague, Netherlands, 2015; available at http://edgar.jrc.ec.europa.eu/news_docs/jrc-2015-trends-in-global-co2-emissions-2015-report-98184.pdf (accessed 17 January 2016).
4. S. Q. Li, L. B. Ma, W. Wan and Q. Yao: 'A mathematical model of heat transfer in a rotary kiln thermo-reactor', Chem. Eng. Technol., 2005, **28**, (12), 1480–1489.
5. K. S. Mujumdar and V. V. Ranade: 'Simulation of rotary cement kilns using a one dimensional model', Chem. Eng. Res. Des., 2006, **84**, (3), 165–177.
6. M. A. Romero Valle: 'Numerical modelling of granular beds in rotary kilns', MSc thesis, Delft University of Technology, Delft, Netherlands, 2012.

7. P. Koukkari: ‘Advanced Gibbs Energy Methods for Functional Materials and Processes’, Research Notes 2506, VTT Technical Research Centre of Finland, Vuorimiehentie, Finland, 2009.
8. P. V. Barr: ‘Heat transfer processes in rotary kilns’, PhD thesis, The University of British Columbia, British Columbia, Canada, 1986.
9. S. H. Tscheng: ‘Convective heat transfer in a rotary kiln’, PhD thesis, The University of British Columbia, British Columbia, Canada, 1978.
10. B. J. McBride, M. J. Zehe and S. Gordon:’ NASA Glenn coefficients for calculating thermodynamic properties of individual species’, National Aeronautics and Space Administration, John H. Glenn Research Center at Lewis Field, Cleveland, Ohio, United States, 2002.
11. J. L. Haas Jr, G. R. Robinson Jr and B. S. Hemingway: ‘Thermodynamic tabulations for selected phases in the system CaO-Al2O3-SiO2-H2 at 101.325 kPa (1 atm) between 273.15 and 1800 K’, J. Phys. Chem. Ref. Data., 1981, **10**, (3), 575–670.
12. E. Mastorakos, A. Massias, C. D. Tsakiroglou, D. A. Goussis, V. N. Burganos and A. C. Payatakes: ‘CFD predictions for cement kilns including flame modelling, heat transfer and clinker chemistry’, Appl. Math. Model., 1999, **23**, (1), 55–76.
13. J. K. Brimacombe and A. P. Watkinson: ‘Heat transfer in a direct-fired rotary kiln: I. Pilot plant and experimentation’, Metall. Trans. B., 1978, **9**, (2), 201–208.
14. P. V. Barr, J. K. Brimacombe and A. P. Watkinson: ‘A heat- transfer model for the rotary kiln: Part II. Development of the cross section model’, Metall. Trans. B., 1989, **20**, (3), 403–419.
15. C. Andersson: ‘Assimulo: a new Python based class for simulation of complex hybrid DAEs and its integration in JModelica.org’, MSc thesis, Lund University, Lund, Sweden, 2011.
16. L. H. J. Wachters and H. Kramers: ‘The calcining of sodium bicarbonate in a rotary kiln’, Proc. 3rd. Eur. Sym. Chem. React. Eng., 1964, **77**.
17. G. W. J. Wes, A. A. Drinkenburg and S. Stemerding: ‘Heat transfer in a horizontal rotary drum reactor’, Powder Technol. 1976, **13**, (2), 185–192.
18. J. M. Lehmberg, M. Hehl and K. Schügerl: ‘Transverse mixing and heat transfer in horizontal rotary drum reactors’, Powder Technol. 1977, **18**, (2), 149–163.
19. E. U. Schluender: ‘Heat transfer to packed and stirred beds from the surface of immersed bodies’, Chem. Eng. Process., 1984, **18**, (1), 31–53.
20. P. V. Barr, J. K. Brimacombe and A. P. Watkinson: ‘A heat- transfer model for the rotary kiln: Part I. Pilot kiln trials’, Metall. Trans. B., 1989, **20**, (3), 391–402.
21. R.A. Svehla: ‘Transport coefficients for the NASA Lewis chemical equilibrium program’, Vol. 4647, 1995, United States, National Aeronautics and Space Administration, Office of Management, Scientific and Technical Information Program.
22. C. M. Harris: ‘Dictionary of architecture and construction’, 2005, New York, United States, McGraw-Hill Professional.

23. R. W. Powell, C. Y. Ho and P. E. Liley: 'Thermal conductivity of selected materials', No. NSRDS-NBS-8, National Bureau of Standards, Washington D. C., United States, 1966.

24. Y. G. Yoon, R. Car, D. J. Scrolovitz and S. Scandolo: 'Thermal conductivity of crystalline quartz from classical simulations', Phys. Rev. B., 2004, **70**, (1), 012302.

25. H. C. Hottel and A. F. Sarofim: 'Radiative transfer', 1967, New York, United States, McGraw-Hill.

26. D.W. Green and R. H. Perry: 'Perry's chemical engineers' handbook', 8th edition, 2008, New York, United States, McGraw-Hill.

27. J. P. Gorog, J. K. Brimacombe and T.N. Adams: 'Radiative heat transfer in rotary kilns', Metall. Trans. B., 1981, **12**, (1), 55–70.

28. K. E. Peray and J. J. Waddell: 'The rotary cement kiln', 1986, London, United Kingdom, Chemical Publishing Company.

29. J. P. Holman: 'Heat transfer', 10th edition, 2010, Boston, Massachusetts, United States, McGraw-Hill.

30. T. Hanein, I. Galan, A. Elhoweris, S. Khare, S. Skalamprinos, G. Jen, M. Whittaker, M. S. Imbabi, F. P. Glasser, and M. N. Bannerman. 'Production of belite calcium sulfoaluminate cement using sulfur as a fuel and as a source of clinker sulfur trioxide: pilot kiln trial', Adv. Cem. Res., 2016, **28**, (10), 643-653.

31. T. Hanein, F. P. Glasser and M. N. Bannerman: 'Thermodynamics of Portland cement clinkering', Proc. 14th. Int. Cong. Chem. Cement, 2015, Beijing, China.

Figure and Table Captions

Figure 1. An illustration of the heat transfer fluxes per length, *Q*, considered in the kiln model. Arrows indicate the positive direction of heat flux. The superscripts indicate convective (cv), radiative (rd), or conductive (cd) terms whereas the subscripts indicate the phases in question: e.g., solid bed (s), gas (g), kiln internal wall (w), and external environment (ext).

Figure 2. The temperature profile along the length of the kiln as obtained from simulation (lines) and Barr trial T4 experiments (symbols). Black solid vertical lines represent the region used for validation of the model.

Figure 3. The temperature profile along the length of the kiln as obtained from simulation (lines) and Tscheng trial A11 experiments (symbols). Black solid vertical lines represent the region used for validation of the model. The region between 1.02m and 1.22m is uninsulated and as the physical properties of the kiln in this region are not known, due to the unknown properties of the equipment installed in that section of the kiln, the initial conditions to perform the integration on either side of this region are calculated separately.

Figure 4. Comparison of the heat fluxes of the various heat transfer paths of Barr trial T4, as predicted by the computational model.

Figure 5. Comparison between the total calculated radiative and convective heat transfer from the gas to both the solid and wall within the kiln enclosure of Barr trial T4.

Table 1. Gaseous composition of dry air used in simulations in this work.

Table 2. Properties of the Tscheng and Barr experimental kilns.

Table 3. A summary of model error for all available experimental data.

Tables

Table 1. Gaseous composition of dry air used.

Component	N_2	O_2	Ar	CO_2	Ne	He	CH_4	Kr
mol-%	78.084	20.946	0.934	3.97×10^{-2}	1.818×10^{-3}	5.24×10^{-4}	1.79×10^{-4}	1.14×10^{-4}

Table 2. Properties of the Tscheng and Barr experimental kilns.

Property	**Barr kiln [8]**	**Tscheng kiln [9]**
Length (m)	5.5	2.44
Inner radius (mm)	205.5	94.25
Refractory thickness (mm)	93.0	1.0
Steel thickness (mm)	6.0	6.35
Ceramic paper thickness (mm)	…	6.4
Fibre glass thickness (mm)	…	76
Outer radius (mm)	304.5	184.0
Experiment IDs	T1—T9	A11—A54

Table 3. Statistics on the deviation from the experimental results of the model temperature predictions for all trial data sets.

Kiln	**Trials**	**Total measurements**			**Maximum error (K)**			**Mean error (K)**		
		Gas	**Solid**	**Wall**	**Gas**	**Solid**	**Wall**	**Gas**	**Solid**	**Wall**
Barr	9	68	73	69	±54.1	±37.8	±39.6	±15.5	±13.9	±13.5
Tscheng	44	88	88	44	±8.6	±17.0	±23.1	±2.2	±3.8	±6.5

Colour figure 1

Click here to download Colour figure (online only) Figure1.eps

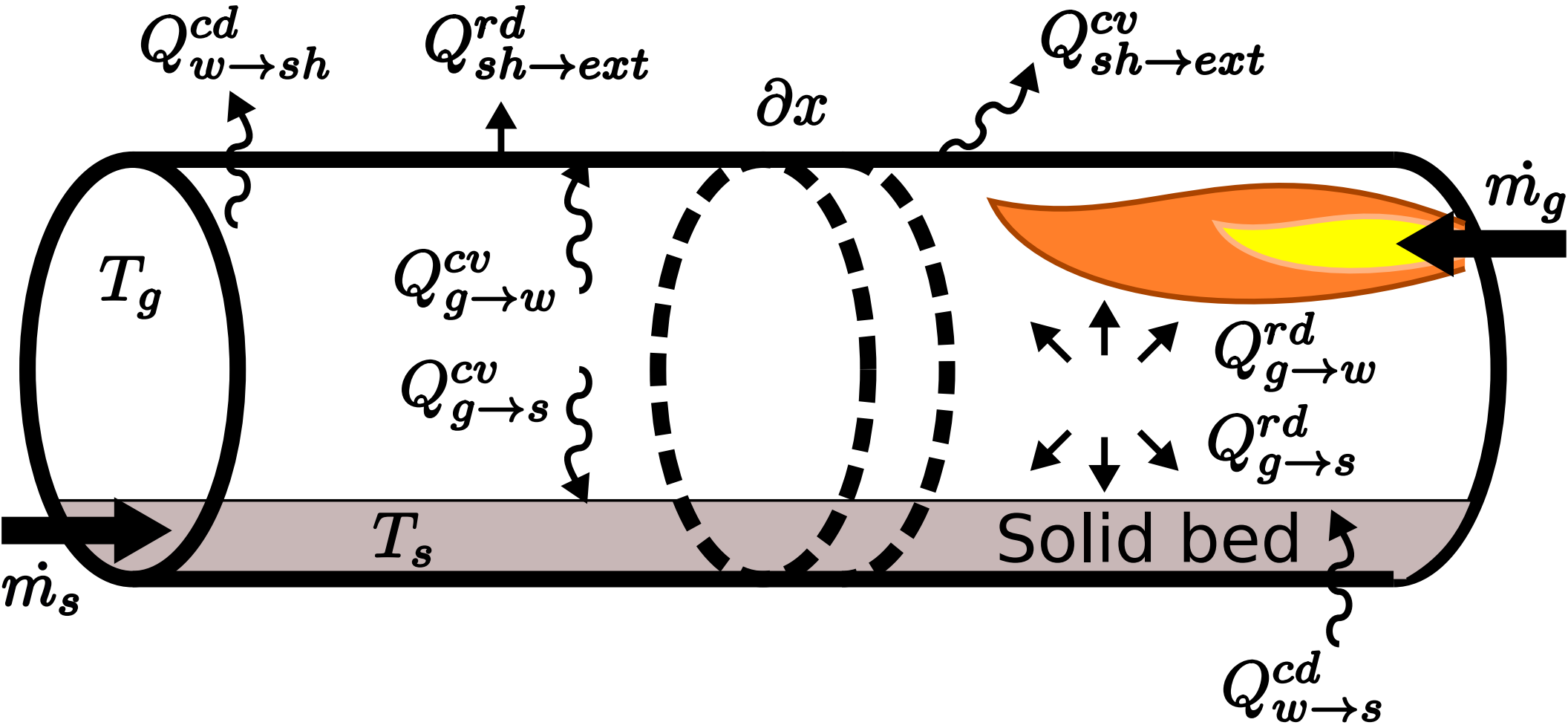

Colour figure 2

Click here to download Colour figure (online only) Figure2.eps

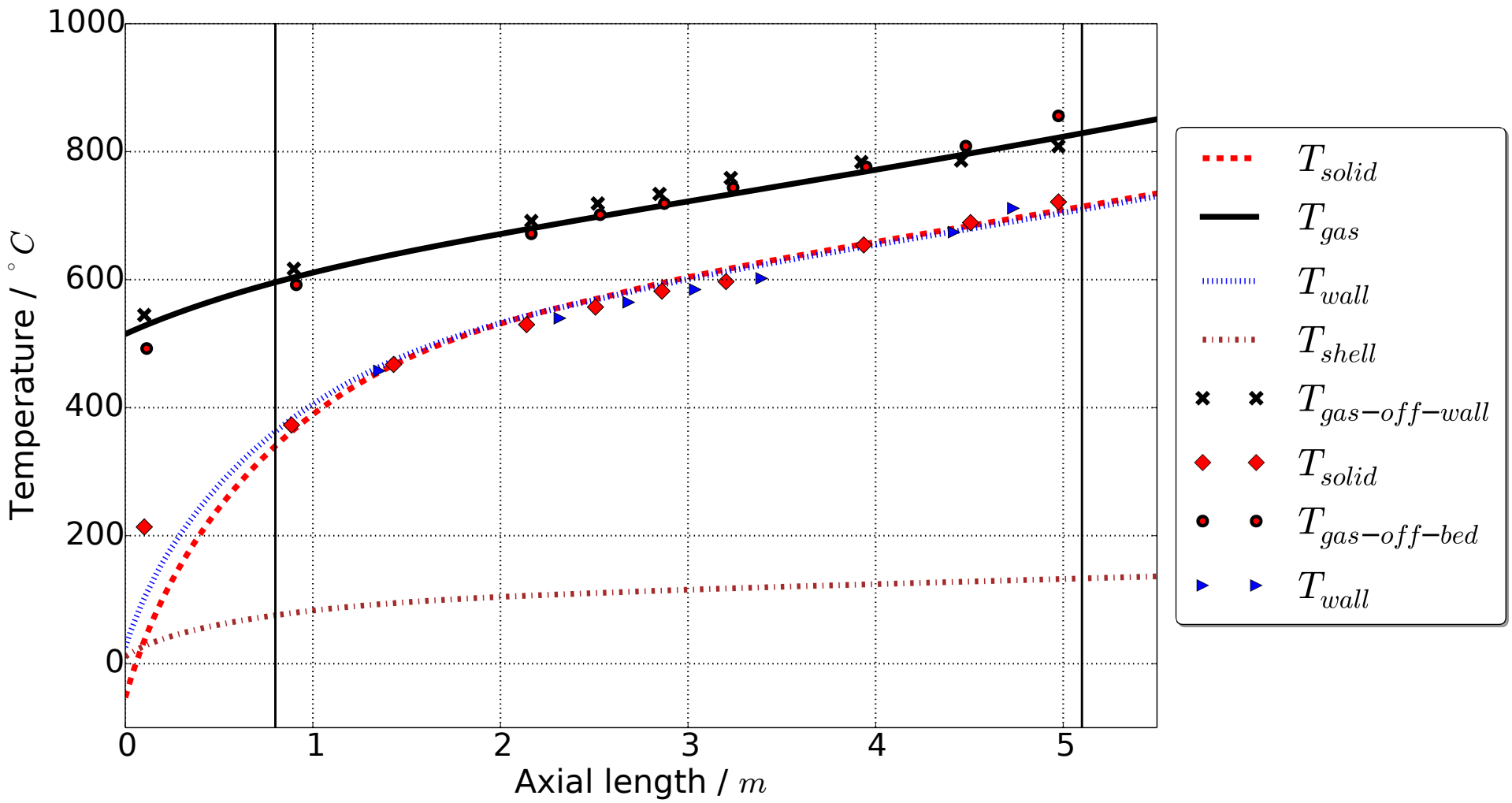

Colour figure 3

Click here to download Colour figure (online only) Figure3.eps

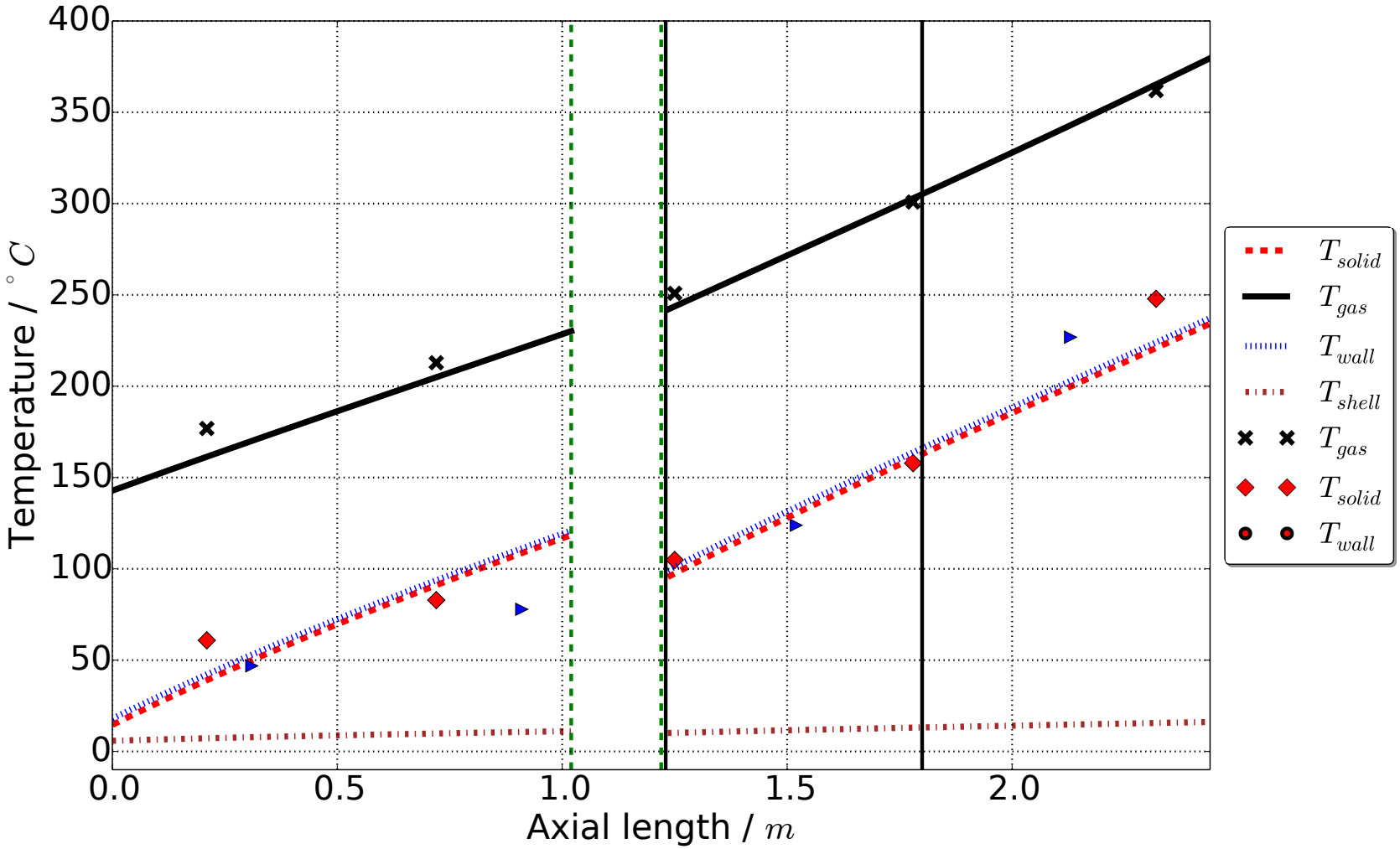

Colour figure 4

Click here to download Colour figure (online only) Figure4.eps

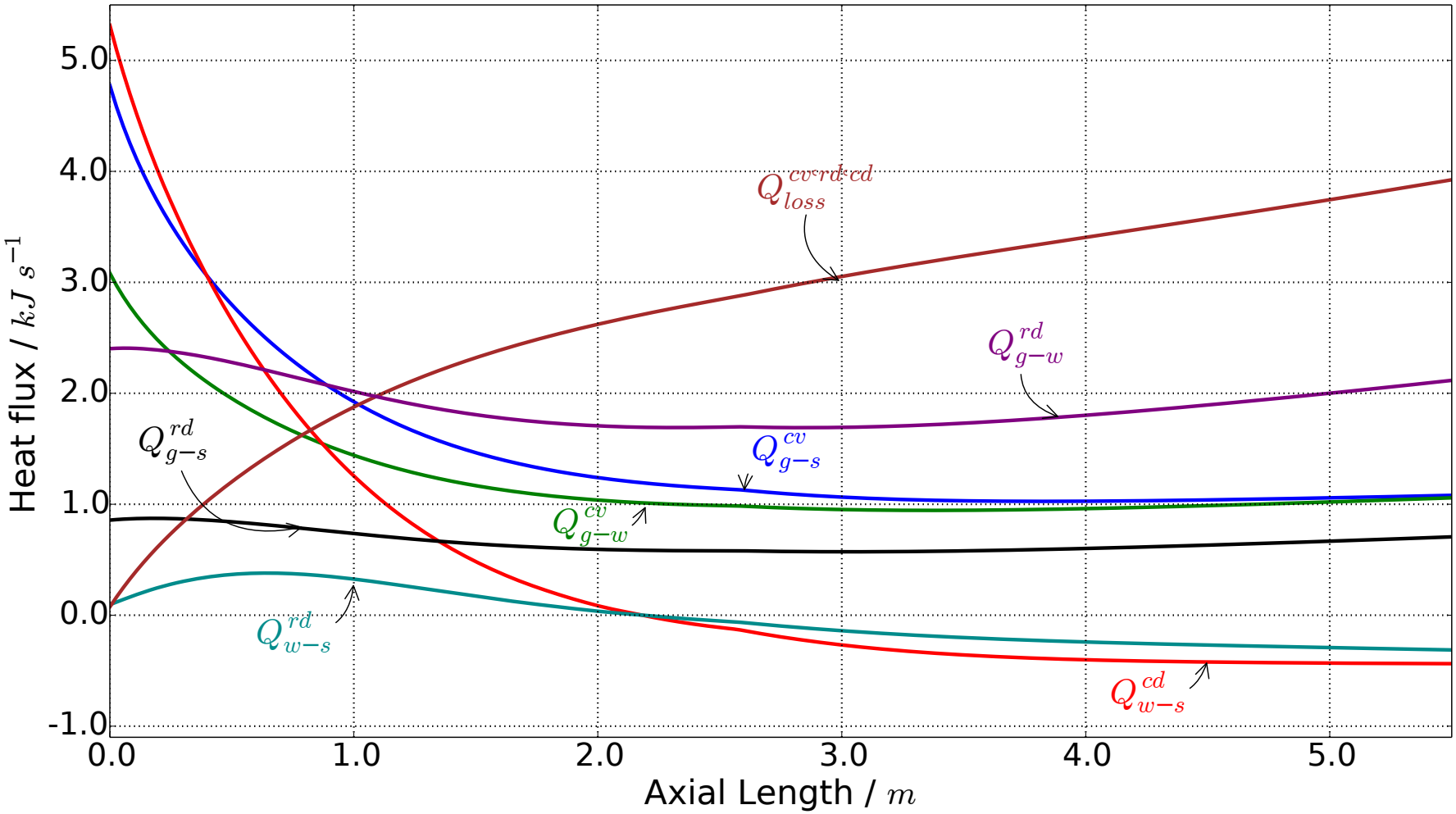

Colour figure 5

Click here to download Colour figure (online only) Figure5.eps

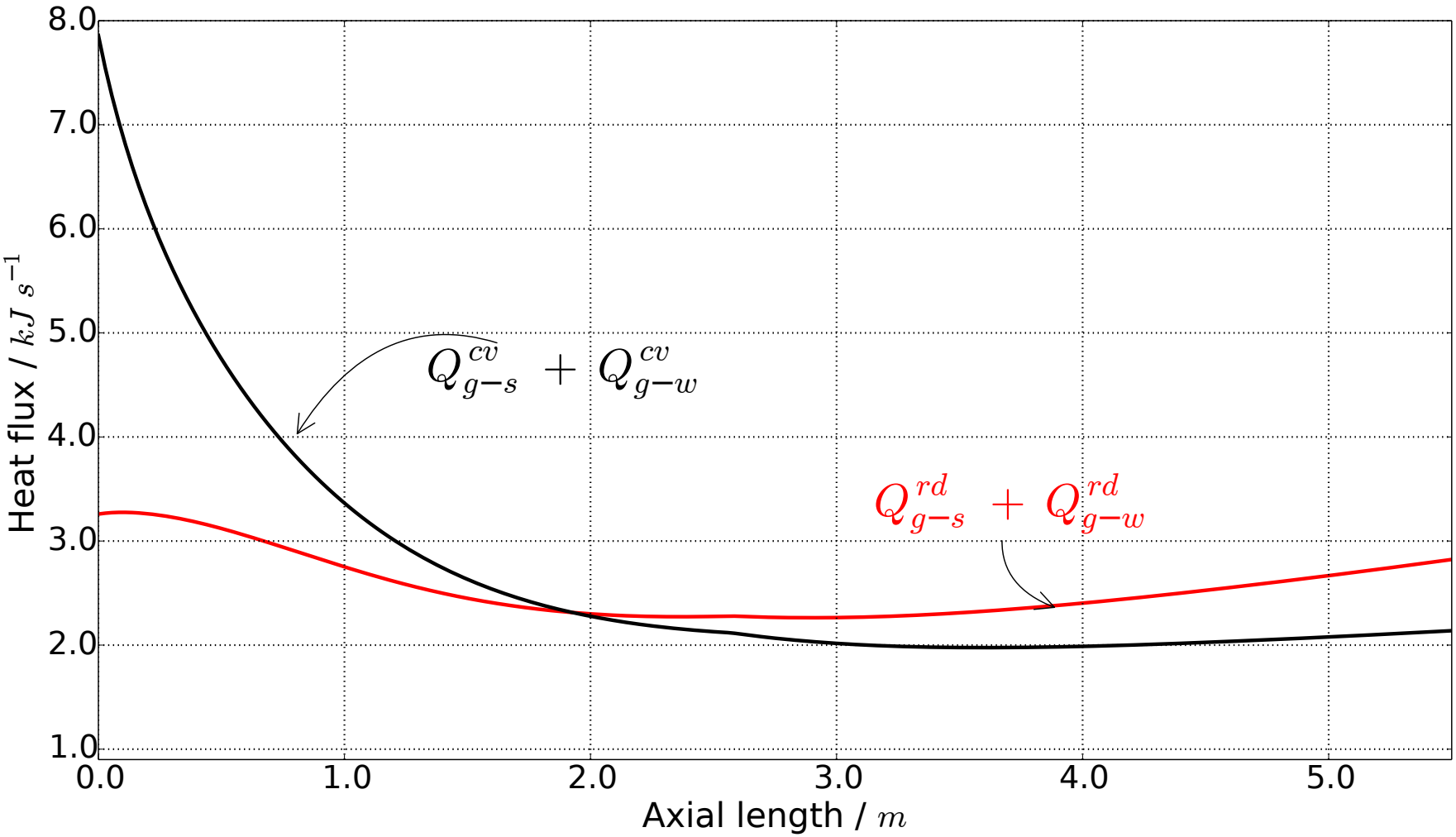

This document provides a description of the supplementary data files provided with the title paper ("1D thermal model of rotary kilns used in cement production").

Supplementary Material 1: Operating conditions of the Tscheng pilot kiln experiments.

Provided in this file are the operating conditions for the 44 Tscheng experiments (A11 – A54) including the air flow-rates, kiln RPM, kiln incline, solid loading, and solid flow-rates. The column labels are in the first row and the units are provided in brackets. The solid particle diameters in all the Tscheng experiments are 0.73 mm.

Supplementary Material 2: Operating conditions of the Barr pilot kiln experiments.

Provided in this file are the operating conditions for the 9 Barr experiments (T1 – T9) including the natural gas flow-rates, primary and secondary air flow-rates, solid flow-rates, and solid particle diameter. The columns labels are in the first row and the units provided in brackets. In all 9 experiments, the solid loading is set at 12% and the kiln RPM set at 1.5.

Supplementary Material 3: Experimental temperature vs kiln length data of the Tscheng pilot kiln experiments.

Provided in this file are the experimental thermocouple temperature measurements for the 44 Tscheng experiments (A11 – A54) taken from the original source. The experiments IDs are given in the first column. The remaining columns contain the thermocouple temperature measurements in Kelvin; these are labelled T-A-B where A denotes the material in question (g for gas, s for solid bed, and w for wall) and B denotes the thermocouple number. The locations of the gas and bed thermocouples are: (1) 0.21, (2) 0.72, (3) 1.25, (4) 1.78, and (5) 2.32 meters along the kiln. The locations of the wall thermocouples are: (1) 0.31, (2) 0.91, (3) 1.52, and (4) 2.13 meters along the kiln. For the thermocouple locations, 0 meters corresponds to the solid feed end of the kiln.

Supplementary Material 4: Experimental temperature vs kiln length data of the Barr pilot kiln experiments.

Provided in this file are the digitized experimental thermocouple temperature measurements (in Kelvin) and locations on the kiln length in meters of the thermocouples for the 9 Barr experiments (T1 – T9). Two sets of gas temperature measurements were collected, one 10 cm off the kiln wall, labelled Tg_off_wall, and the second, 2.5 cm off the kiln solid bed labelled Tg_off_bed, both from the same thermocouple measured as the kiln rotates. The solid bed and wall temperature measurements are labelled Ts and Tw respectively. The thermocouples are fixed therefore their locations are assumed to be the average of the digitized measurements. The numbers following column headers denote the thermocouple numbers. The gas thermocouple locations are: (1) 0.11, (2) 0.89, (3) 2.15, (4) 2.51, (5) 2.85, (6) 3.20, (7) 3.91, (8) 4.44, and (9) 4.95. The solid bed thermocouple locations are: (1) 0.11, (2) 0.87, (3) 1.44, (4) 2.14, (5) 2.50, (6)

2.85, (7) 3.20, (8) 3.91, (9) 4.48, (10) 4.95, (11) 5.25, and (12) 5.50 meters. The wall thermocouple locations are: (1) 1.33, (2) 2.32, (3) 2.67, (4) 3.03, (5) 3.38, (6) 3.83, (7) 4.40, and (8) 4.78. For the thermocouple locations, 0 meters represents the solid feed end of the kiln. Data shown as “NA” in this file implies that data are not available for that thermocouple.

Supplementary Material 1

Experiment ID	Air flow (kg/hr)	RPM	Incline (degree)	Solid loading (%)	Solid flow (kg/hr)
A11	24.6	3	1.2	17	25
A12	24.6	3	1.2	17	25
A13	24.6	3	1.2	17	25
A14	24.6	3	1.2	17	25
A15	24.6	1.5	1.2	17	14.2
A16	24.6	1.5	1.2	17	14.2
A17	24.6	1.5	1.2	17	14.2
A18	18.6	3	1.2	15	21
A19	18.6	1.6	2.2	17	29.1
A20	18.6	1.6	1.2	17	15
A21	34	1.5	1.2	17	15
A22	34	3	1.2	17	34
A23	34	1.5	1.2	17	15
A24	34	6	1.2	17	50.5
A25	34	1.5	3.4	17	39
A26	34	3.2	2.2	11	34.6
A27	50.5	3.2	2.2	11	34
A28	50.5	3.1	3	11	52.7
A29	50	3.1	1.2	11	19.4
A30	50	1.6	2.2	11	18.2
A31	50.5	6	2.2	11	66.3
A32	81	3	2	11	36
A33	65.5	3	2	11	36
A34	73	3	2	11	36
A35	81	3	2	11	36
A36	34	3	2	11	36
A37	34	3	2	11	36
A38	34	3	2	11	36
A39	34	3	2	11	36
A40	18.6	3	2	11	36
A41	18.6	3	2	11	36
A42	18.6	3	2	11	36
A43	18.6	3	2	11	36
A44	50	3	2	11	36
A45	65.5	0.9	2	6.5	12
A46	34	1	2	6.5	13.3
A47	34	3	2	6.5	35.8
A48	65.5	3	2	6.5	35.8
A49	65	0.9	2	6.5	11.7
A50	95.5	3	2	6.5	35.8
A51	95.5	1	2	6.5	15.8
A52	34	1	2	6.5	11.3
A53	95.5	1	2	6.5	16.1
A54	81	0.95	2	6.5	12

Click here to download Datasets Supplementary Material 2.xls

Experiment ID	Fuel flow rate (L/s)	Primary air flow rate (L/s)	Secondary air flow rate (L/s)
T1	0.83	9.4	18.8
T2	1.02	16.5	40.6
T3	1.42	17.4	40.6
T4	1.97	17.4	43
T5	0.68	9.4	19.8
T6	0.9	14.2	29.3
T7	1.04	18.4	43
T8	2	18.8	40.1
T9	2.53	18.8	43

Solid mass flow rate (kg/hr)	Sand Particle Diameter (mm)
62	2.5
62	2.5
62	2.5
62	2.5
58	0.58
62	0.58
63	0.58
64	0.58
65	0.58

 Click here to download Datasets Supplementary Material 3.xls

Experiment ID	T-g-1	T-g-2	T-g-3	T-g-4	T-g-5	T-s-1	T-s-2	T-s-3
A11	450	486	524	574	635	334	356	378
A12	425	460	489	535	592	323	339	356
A13	402	423	457	493	538	321	337	354
A14	372	392	411	436	457	314	327	341
A15	330.6	340	348.3	358.8	372	306.7	308.9	312.8
A16	414	438	462	494	535	341	356	374
A17	470	505	543	594	652	364	383	410
A18	351.5	378.9	412.2	445	488	313.9	325.6	338.9
A19	350	375.1	405	448	497	312.2	322.2	332.2
A20	365	392.8	427.2	464	507	330.5	340	352.8
A21	380	398	418	436	455	335	346.1	360.3
A22	368	388	407	428	455.8	320.6	331.1	341.7
A23	383	400.8	418	437	456	337.8	348.9	365
A24	357	374	390.6	407	430	308.3	315	322.2
A25	361	377.2	391.5	410	430	305.6	313.6	322.2
A26	370	385	398.9	414	437	313.8	323.3	333.3
A27	369	380	388.9	401	413	316.7	326.1	334.4
A28	361	371	381.1	395	410	312.8	318.9	327.9
A29	376	386	396	406	417	328.9	339.4	353.9
A30	378	388	399	410	420.5	329.4	341.1	357.2
A31	353	365	375.6	387.5	404.5	308.3	313.9	321.5
A32	407	417.8	425.1	437.5	450	333.3	350.6	366.7
A33	393	407	418.3	431	445	326.1	341.7	358.3
A34	396.2	412.2	423.3	436	448.9	331.7	347.2	362.7
A35	396.8	411.1	422.2	433	444.4	326.7	348.9	366.7
A36	366.7	380.6	395.6	415	441	311.1	322.2	334.4
A37	420	445.4	476.7	513	560	322.8	343.3	369.4
A38	395	417	440.6	471	505	318.9	334.4	355
A39	420.6	446.5	475	512	559	323.9	343.3	369.4
A40	385.6	417	461.1	510	560	318.3	331.7	352
A41	358.3	376	410.6	447	505	308.9	317.8	332.2
A42	351.7	360	384.4	413.5	460	306.1	312.2	321.7
A43	375.6	400	440	478	535	313.3	325	345
A44	398	416.7	433.9	452.5	475	323.9	338.9	360
A45	412	425	434.4	441.1	448	361.1	373.9	391.7
A46	382.1	397.2	413.3	427.3	444	333.3	345.6	361.7
A47	367.8	382.2	398.9	416	441	312.8	322.8	336.1
A48	400	408	420.6	432	447	327.8	341.1	360
A49	419	427	435	442.3	448	368.9	378.3	397.8
A50	404	410.2	417.2	424	431	375	377.8	391.7
A51	406.6	412.2	417.6	422	427	370.6	377.2	390.6
A52	384	398.1	416.7	428	443	335.5	348.9	368.3
A53	403.3	409.5	414.4	413.5	422.8	374.4	375.6	388.9
A54	419	427	434.4	442	450	373.3	381.7	397.2

T-s-4	T-s-5	T-w-1	T-w-2	T-w-3	T-w-4
431	521	320	351	397	500
397	473	314	338	372	445
392	447	313	333	368	429
368	405	308	326	352	395
326.7	348.3	301	306	316	333
417	473	324	347	387.5	447
473	554	341	370	425	520
363.9	402.8	308	323	349	385
355.5	391.7	304	317	341	377
383.3	424.4	315.5	331	363	407
384.4	411.1	319.4	336	365.8	401
363.3	390	311	326.6	349.6	378
385.6	412.8	321	338	365	400
336.7	360	302	311.6	330	355
338.9	362.1	300	313.4	331	360
350	376.1	306	321.6	340	364.8
351.7	373.9	306.8	323	341.6	366
341.7	358.9	304	315.5	333	353
370.6	391.1	320	338.8	350	380
373.9	394.4	320	339	360	387
331.7	350	302.3	313.6	326	345.6
391.1	417.3	321.1	347.4	375.5	407
380.6	407.2	313	338.4	367.4	395
385.8	412.2	315.8	344	370	402
388.9	414.2	315.8	345	375.5	404
352.2	378.1	304.5	321.7	339	368
399.7	443	312.6	341.1	380.4	425.5
380	415.3	312.4	335.4	361	401
400	445.4	312	344	380	425.5
377.8	428	311	333	364	413
348.3	387.2	300.4	317.6	335	372.8
336.1	366.7	299	312.6	327	356.8
365	412.2	306	325	352	397.5
384.2	419.4	312	338	371	407
416.7	434.4	339.8	365	400	428
386.7	411.1	314	338.4	369.4	400
352.8	380	306	323.6	344.2	370.5
382	409.4	318	340.2	369	395
419.4	438.3	349.6	374.4	402.5	430
407.2	418.9	355	374	395	415
402.7	418.3	351.4	372.2	393.3	413
391.7	418.9	319	341.5	373	405
404.4	415.6	347	369	395	410
418.9	435	351	364.4	400	430

Supplementary Material 4 Click here to download Datasets Supplementary Material 4.xls

Experiment ID	T1	T2	T3	T4	T5
Tg_off_wall 1	592.996	612.5	701.567	817.842	585.573
Tg_off_wall 2	661.964	660.714	765.204	890.041	640.609
Tg_off_wall 3	749.991	707.143	824.451	964.73	714.213
Tg_off_wall 4	769.207	726.786	837.618	992.116	735.246
Tg_off_wall 5	803.748	726.786	848.589	1007.05	749.782
Tg_off_wall 6	818.617	744.643	855.172	1031.95	770.839
Tg_off_wall 7	872.36	757.143	890.282	1056.85	808.566
Tg_off_wall 8	NA	771.429	NA	1059.34	818.314
Tg_off_wall 9	943.188	787.5	907.837	1081.74	836.834
Tg_off_bed 1	564.547	589.286	673.041	765.56	557.191
Tg_off_bed 2	576.646	619.643	730.094	865.145	570.781
Tg_off_bed 3	629.676	687.5	795.925	944.813	613.845
Tg_off_bed 4	662.016	707.143	815.674	974.689	643.628
Tg_off_bed 5	692.196	716.071	833.229	992.116	675.591
Tg_off_bed 6	744.25	NA	848.589	1017.01	727.188
Tg_off_bed 7	848.3	757.143	NA	1049.38	778.003
Tg_off_bed 8	891.362	764.286	894.671	1081.74	800.863
Tg_off_bed 9	927.877	783.929	NA	1129.05	808.476
Ts1	400.487	371.429	464.577	486.722	400.107
Ts2	454.172	NA	574.295	646.058	453.009
Ts3	514.676	528.571	642.32	740.664	NA
Ts4	555.323	NA	688.401	802.905	509.162
Ts5	NA	591.071	712.539	830.29	538.921
Ts6	606.878	NA	725.705	855.187	553.41
Ts7	NA	NA	749.843	870.124	587.555
Ts8	NA	650	778.37	927.386	640.552
Ts9	751.305	673.214	806.897	962.241	685.131
Ts10	809.75	700	857.367	994.606	701.588
Ts11	NA	NA	815.674	NA	735.828
Ts12	854.971	730.357	852.978	NA	768.005
Tw1	530.129	535.714	626.959	730.705	504.345
Tw2	587.89	583.929	694.984	812.863	563.319
Tw3	609.293	601.786	714.734	837.759	584.375
Tw4	635.099	616.071	732.288	857.676	603.227
Tw5	652.128	628.571	749.843	875.104	624.284
Tw6	704.025	651.786	789.342	NA	662.579
Tw7	764.543	687.5	822.257	947.303	694.069
Tw8	812.15	712.5	850.784	984.647	732.483

T6	T7	T8	T9
673.041	651.066	834.648	874.748
690.596	659.607	876.944	966.177
747.649	703.487	959.68	1072.98
756.426	709.999	974.382	1090.49
776.176	716.512	1010.67	1116.66
780.564	725.246	1031.86	1136.34
813.48	742.71	1059.12	1173.51
802.508	742.469	NA	NA
802.508	755.581	1105.45	1219.5
585.266	582.173	741.92	805.349
642.32	628.497	838.121	924.972
727.9	690.144	935.95	1044.8
747.649	701.106	963.601	1070.97
760.815	705.43	989.108	NA
NA	NA	NA	NA
795.925	729.372	1046.18	1173.51
787.147	NA	NA	1178.08
787.147	744.47	1120.55	1252.04
365.831	428.843	450.82	503.907
484.326	504.06	618.199	701.579
541.379	530.475	712.463	797.252
585.266	550.161	780.714	882.137
605.016	572.224	810.51	921.324
618.182	587.62	823.068	951.841
640.125	605.248	857.199	978.025
668.652	629.374	903.877	1023.87
694.984	660.229	950.693	1076.17
727.9	662.244	995.478	1126.25
NA	NA	NA	NA
NA	684.235	NA	NA
565.517	534.963	710.422	803.711
620.376	581.195	791.3	901.731
637.931	598.813	818.951	938.754
653.292	609.765	837.977	962.765
662.069	618.5	865.629	995.45
694.984	644.968	912.582	1041.19
714.734	NA	NA	1071.79
738.871	684.538	987.026	1113.17